Environmental Science and Pollution Research (2020) 27:11127–11137
https://doi.org/10.1007/s11356-020-07752-1

RESEARCH ARTICLE

Novel reduced graphene oxide/$ZnBi_2O_4$ hybrid photocatalyst for visible light degradation of 2,4-dichlorophenoxyacetic acid

Nguyen Thi Mai Tho[1] · Dang Nguyen Nha Khanh[2,3] · Nguyen Quoc Thang[1] · Yong-Ill Lee[3] · Nguyen Thi Kim Phuong[2,4]

Received: 3 October 2019 / Accepted: 14 January 2020 / Published online: 18 January 2020

Abstract

A new highly efficient rGO/$ZnBi_2O_4$ hybrid catalyst has been successfully synthesized through oxidation-reduction and co-precipitation methods, followed by heating at 450 °C. The obtained rGO/$ZnBi_2O_4$ catalyst was characterized by X-ray diffraction (XRD), UV-vis diffuse reflectance spectroscopy (DRS), scanning electron microscopy (SEM), Fourier-transform infrared (FTIR) spectroscopy, and X-ray photoelectron spectroscopy (XPS). The catalytic activity of rGO/$ZnBi_2O_4$ under visible light irradiation was tested using 2,4-dichlorophenoxyacetic acid (2,4-D) in aqueous solution. The rGO/$ZnBi_2O_4$ hybrid catalyst containing 2% rGO (2.0rGO/$ZnBi_2O_4$) showed the best catalytic performance. More than 90% of 2,4-D in a 30 mg/L solution was degraded after 120 min of visible light irradiation using 2.0rGO/$ZnBi_2O_4$ at 1.0 g/L concentration. Moreover, the 2.0rGO/$ZnBi_2O_4$ catalyst showed excellent stability over four consecutive cycles, with no significant changes in the photocatalytic degradation rate. This study demonstrated that rGO/$ZnBi_2O_4$ may be a promising, low-cost, and green photocatalyst for environmental remediation applications.

Keywords rGO/$ZnBi_2O_4$ hybrid catalyst · 2,4-Dichlorophenoxyacetic acid · Visible light irradiation · Photodegradation · Kinetic

Introduction

Water contamination by agrochemicals is a cause of growing concern, due to potential environmental damage. Among numerous agrochemicals in use today, the 2,4-dichlorophenoxyacetic acid (2,4-D) herbicide is widely used to control broadleaf weeds. After application, 2,4-D is easily transported into natural waters, due to its high solubility. The herbicide is very toxic, persistent, and difficult to biodegrade, and accumulates in the environment, thus posing a potential danger to human and aquatic life.

For an efficient treatment of water contaminated with organic pollutants, a number of advanced oxidation processes (AOPs), including photo-Fenton (An et al. 2013; Huy et al. 2017a, 2019; Wang and Chu 2012), photocatalytic (An et al. 2015; Peng et al. 2014), and electrochemical oxidation (Martínez-Huitle and Ferro 2006) are currently in use or under study. Photocatalysis is a good alternative for the degradation of organic pollutants. The pollutants can be effectively degraded by active species such as photoinduced holes as well as hydroxyl and superoxide radicals, which are formed in heterogeneous photocatalysts under appropriate light irradiation. (Ponraj et al. 2017) Photocatalysts exhibit outstanding features including non-toxicity and excellent stability for repeated use. A number of new semiconductors based on bismuth, such as Bi_2S_3 (Cao et al. 2012; Wang et al. 2017), Bi_2O_3 (Cheng and Kang 2014; Peng et al. 2014; Xu et al. 2012; Yang et al. 2014), BiOCl (Cao et al. 2012), $BiFeO_3$ (An et al. 2013; Gadhi et al. 2018; Ponraj

Nguyen Thi Mai Tho and Dang Nguyen Nha Khanh are co-first authors.

Responsible editor: Suresh Pillai

✉ Yong-Ill Lee
yilee@changwon.ac.kr

✉ Nguyen Thi Kim Phuong
nguyenthikimp@yahoo.ca

[1] Chemical Engineering Faculty, Industrial University of Ho Chi Minh City, Ho Chi Minh City, Vietnam

[2] Hochiminh city Institute of Resources Geography, Vietnam Academy of Science and Technology, 01 Mac Dinh Chi, District 1, Ho Chi Minh City, Vietnam

[3] Department of Chemistry, Changwon National University, Changwon 641-773, South Korea

[4] Graduate University of Science and Technology, Vietnam Academy of Science and Technology, 18 Hoang Quoc Viet, Cau Giay, Hanoi, Vietnam

et al. 2017), $BiVO_4$ (Ju et al. 2014; Tokunaga et al. 2001; Yu and Kudo 2006), and $BiWO_6$ (Ju et al. 2014; Wu et al. 2008; Zhao et al. 2012) have attracted increasing attention and have been extensively studied as visible light-active photocatalysts. Mixed-metal oxides derived from double-layered hydroxides (LDHs) are currently receiving considerable attention in the catalysis field. LDHs are two-dimensional (2D)-layered anionic clays, generally formulated as $[M_{1-x}^{2+}M_x^{3+}(OH)_2]^{x+}(A^{n-})_{x/n};yH_2O$ (where M^{2+} and M^{3+} are divalent and trivalent metals, respectively, and A^{n-} is an interlayer anion) (Goh et al. 2008; Mishra et al. 2018; Mohapatra and Parida 2016). As one of the simplest mixed-metal oxides, $ZnBi_2O_4$ is a promising visible light catalyst, due to the internal electric field generated at the junction created between ZnO and Bi_2O_3. Numerous studies focused on the application of $ZnBi_2O_4$ photocatalysts for the elimination of organic pollutants, using visible light as the irradiation source (Goswami and Ananthakrishnan 2017; Huy et al. 2017b, 2019; Thi Mai Tho et al. 2018; Tho et al. 2018). Graphene is one of the most studied materials. The use of graphene as a co-catalyst continues to attract the attention of the scientific community, due to its large specific surface area, high electron mobility, and excellent chemical stability (Goswami and Ananthakrishnan 2017; Kumar et al. 2015; Pei et al. 2010; Wang et al. 2014; Wu et al. 2012; Yao et al. 2014; Yuan et al. 2015; Zhong et al. 2015). In particular, graphene acts as a good electron acceptor and transporter in composite materials and thus slows down the hole-electron recombination (Meng et al. 2014; Sun et al. 2013). Composite materials based on graphene have been widely reported to show enhanced photocatalytic activity for the degradation of organic pollutants. Coupling two or more semiconductors is known as one of the most effective methods to improve the catalytic activity (Huy et al. 2017a; Ju et al. 2014; Martínez-Huitle and Ferro 2006; Shekofteh-Gohari and Habibi-Yangjeh 2016). The formation of heterojunctions between the semiconductors enhances the separation efficiency and extends the lifetime of photogenerated electrons (e^-) and holes (h^+), resulting in a significantly increase in photocatalytic activity (Goswami and Ananthakrishnan 2017; Yao et al. 2014; Zhong et al. 2015). However, the preparation of these compounds is still a significant challenge. Therefore, photocatalytic studies have focused on identifying simple compounds, as well as improving their visible light sensitivity and photodegradation efficiency for organic pollutants.

This work focused on combining $ZnBi_2O_4$ with reduced graphene oxide (rGO) to produce highly efficient rGO/$ZnBi_2O_4$ hybrid catalysts. The photocatalytic behavior of the rGO/$ZnBi_2O_4$ catalysts was studied by examining the degradation of 2,4-D under visible light irradiation. In addition, we proposed a possible mechanism for the enhanced photocatalytic activity of the rGO/$ZnBi_2O_4$ hybrid.

Experimental

Materials

All chemicals used were analytical grade. Graphite, sulfuric acid (H_2SO_4), nitric acid (HNO_3), hydrogen peroxide (H_2O_2), potassium permanganate ($KMnO_4$), $NaBH_4$, zinc (II) nitrate hexahydrate ($Zn(NO_3)_2.6H_2O$), and 2,4-dichlorophenoxyacetic acid (2,4-D) used for this study were purchased from Sigma-Aldrich. Bismuth (III) nitrate pentahydrate ($Bi(NO_3)_3.5H_2O$) and sodium hydroxide (NaOH) were obtained from Junsei Chemical Co., Japan.

Equipment

The crystalline phases of samples were investigated using a Rigaku Ultima IV X-ray diffractometer (Japan). The measurements were carried out at room temperature with Cu Kα radiation ($\lambda = 1.54051$ Å) at 40 kV and 40 mA were recorded in the region of 2θ from 10° to 50°. Scanning electron microscopy (SEM) micrographs were examined using a Tescan MIRA 3 LM scanning electron microscope (USA) with an accelerating voltage of 20 kV. The UV-vis diffuse reflectance spectra (DRS) were recorded on a Jasco V 550 UV-vis spectrophotometer (Japan). Fourier-transform infrared spectroscopy was recorded by Perkin Elmer FTIR spectrophotometer RXI. Liquid total organic carbon (TOC) of samples was determined with a Shimadzu TOC-VCPH analyzer (Japan). The concentration of inorganic chloride was quantified using a Metrohm 940 Professional Vario ion chromatography (Switzerland). The concentration of 2,4-D was determined with a Thermo Evolution 201 UV-visible spectrophotometer (USA) over the range of 800 to 200 nm using quartz cuvettes.

Synthesis

Preparation of rGO

First, graphene oxide (GO) was prepared by a chemical oxidation method (Akhavan and Ghaderi 2009; Goswami and Ananthakrishnan 2017; Hummers and Offeman 1958). A mixture of graphite and $NaNO_3$ was slowly added to a 500 mL beaker containing 98% H_2SO_4 placed in an ice bath, stirring continuously for 3 h. Then, $KMnO_4$ was carefully added to the suspension, ensuring that the reaction temperature remained below 20 °C. The mixture was then heated to 35 °C and stirred for 2 h to form a thick paste. After that, distilled water was slowly added to the thick paste and stirred continuously for 2 h at 98 °C. Then, more distilled water was added to stop the oxidation reaction. Next, 30% H_2O_2 was added to the above mixture and a yellow color appeared. The obtained graphite oxide was washed with 5% HCl and then with distilled water until pH 7 was reached. Then,

graphite oxide was dispersed in distilled water and exfoliated to produce GO sheets via ultrasonic treatment for 4 h. The GO sheets were collected by centrifugation for 20 min at 4000 rpm and dried in a vacuum oven at 80 °C for 24 h. To obtain rGO, after thoroughly dispersing GO into distilled water, $NaBH_4$ was added to reduce the carboxyl and oxygen functional groups. Next, the mixture was refluxed for 24 h at 100 °C. The rGO sample was obtained by washing with distilled water to pH 7 and drying in a vacuum oven at 80 °C for 24 h.

Preparation of rGO/$ZnBi_2O_4$ hybrid

For the preparation of rGO/$ZnBi_2O_4$ hybrid powders, the rGO obtained as described above was dispersed in distilled water in different percentages ($x = 0$, 1, 2, and 3%) and sonicated for 30 min at 75 ± 5 °C. Then, a solution of $Zn(NO_3)_2{\cdot}6H_2O$ and $Bi(NO_3)_3{\cdot}5H_2O$ in nitric acid (5%) with a molar ratio of 3:1 and an alkaline solution of 1 M NaOH were added dropwise, at a flow rate of 2 mL/min. The pH of the mixture was maintained at 10, and the mixture was stirred for 24 h at 75 ± 5 °C. The precipitate was then obtained by centrifugation and washing with distilled water, followed by drying at 70 °C for 10 h and annealing at 450 °C for 3 h to obtain the rGO/$ZnBi_2O_4$ hybrid powders. The as-prepared powders obtained in this way, containing 0, 1, 2, and 3% of rGO, were labeled $ZnBi_2O_4$, 1.0rGO/$ZnBi_2O_4$, 2.0rGO/$ZnBi_2O_4$, and 3.0rGO/$ZnBi_2O_4$, respectively.

Photocatalytic experiment

The photocatalytic properties of the as-prepared samples were evaluated by monitoring the degradation of 2,4-D under visible light irradiation. The photoreactor was equipped with a 300 W halogen lamp (Osram, Germany). A continuous cold water supply was circulated though the jacket to control a constant temperature of the reaction mixture. Prior to visible light irradiation, the catalyst and 2,4-D solution were allowed to stir in the darkroom for 60 min to establish the adsorption/desorption equilibrium between 2,4-D and the catalyst surface. The reactions were carried out in triplicate, and 5 mL aliquots of the solution were collected at different time intervals for a total of 120 min. The quantity of 2,4-D in solution was traced by measuring the UV-vis absorption (Thermo, USA).

Results and discussion

Characterization of materials

The XRD patterns of rGO, pristine $ZnBi_2O_4$, and rGO/$ZnBi_2O_4$ are shown in Fig. 1a. The XRD pattern of rGO showed a weak and broad diffraction peak centered at 2θ = 24.6°, which can be attributed to the very thin rGO layers due to the high degree of exfoliation. (Pei et al. 2010). As shown in Fig. 1a, all peaks of pristine $ZnBi_2O_4$ matched well with the characteristic reflections of ZnO (2θ = 31.9, 34.7, and 36.5°) corresponding to the powder diffraction files (PDFs) no. 00-079-0207 and Bi_2O_3 (2θ = 25.0, 25.9, 27.8, 30.4, 33.2, 37.2, and 39.7°), corresponding to the standard JCPDS data (No. 00-076-1730 and 00-071-0467). In the case of rGO/$ZnBi_2O_4$, the peaks appeared at 2θ = 27.1 and 28.1° are well matched with the standard JCPDS data (No. 00-076-1730). Most diffraction peaks of rGO/$ZnBi_2O_4$ were similar to those of pristine $ZnBi_2O_4$, however, with a very slight shift from the pristine $ZnBi_2O_4$ possibly due to the formation of a heterojunction between rGO and $ZnBi_2O_4$. All diffraction peaks were relatively sharp and symmetrical, indicating the high crystallinity of the sample.

Figure 1b shows the FTIR spectra of the rGO, pristine $ZnBi_2O_4$, and rGO/$ZnBi_2O_4$ samples. The rGO sample exhibited characteristic vibrational peaks at 1721 and 1230 cm^{-1}, corresponding to the stretching modes of C=O and C–O groups, respectively (Kumar et al. 2015; Wu et al. 2012). The peak at 1574 cm^{-1} in the rGO spectrum can be assigned to the ring skeletal vibration (Yuan et al. 2015). The bands at 1391 and 843 cm^{-1} in the pristine $ZnBi_2O_4$ and rGO/$ZnBi_2O_4$ samples are typically attributed to Bi–O and Bi–O–Bi stretching modes, respectively (Liu et al. 2011a).

Figure 1c shows the UV-vis diffuse reflectance spectroscopy (DRS) data of pristine rGO, $ZnBi_2O_4$, and rGO/$ZnBi_2O_4$. All materials could absorb in the visible region; however, the spectrum of rGO/$ZnBi_2O_4$ showed a red shift compared to that of pristine $ZnBi_2O_4$. This change is due to the hybridization of rGO with $ZnBi_2O_4$, which results in the formation of chemical bonds between rGO and $ZnBi_2O_4$, e.g., Zn–C and Bi–C bonds, in the rGO/$ZnBi_2O_4$ photocatalyst (Liu et al. 2011b; Wang et al. 2014). The band gap energy (E_g) of the samples was estimated using the Tauc plot (Fig. 1c, inset). Pristine $ZnBi_2O_4$ showed two band gap values of 2.90 and 2.25 eV, corresponding to wurtzite ZnO and Bi_2O_3, respectively; on the other hand, the rGO/$ZnBi_2O_4$ sample exhibited a single band gap value, located at 2.90 eV for 2.0rGO/$ZnBi_2O_4$ and at 3.00 eV for 1.0rGO/$ZnBi_2O_4$ and 3.0rGO/$ZnBi_2O_4$.

In order to further investigate the structural characteristics and interfacial features of the as-prepared samples, field-emission SEM (FE-SEM) measurements were carried out; the results are presented in Fig. 2.

The FE-SEM micrographs reveal that the pristine rGO sample exhibited a sheet-like morphology, while pristine $ZnBi_2O_4$ was composed of uneven particles stacked on top of each other. The images of the rGO/$ZnBi_2O_4$ samples show that $ZnBi_2O_4$ was grown on the rGO sheet. This indicates that $ZnBi_2O_4$ was successfully loaded onto the surface of rGO. The energy dispersive spectroscopy (EDS) results confirm that the rGO/$ZnBi_2O_4$ sample consisted of Zn, Bi, C, and O elements.

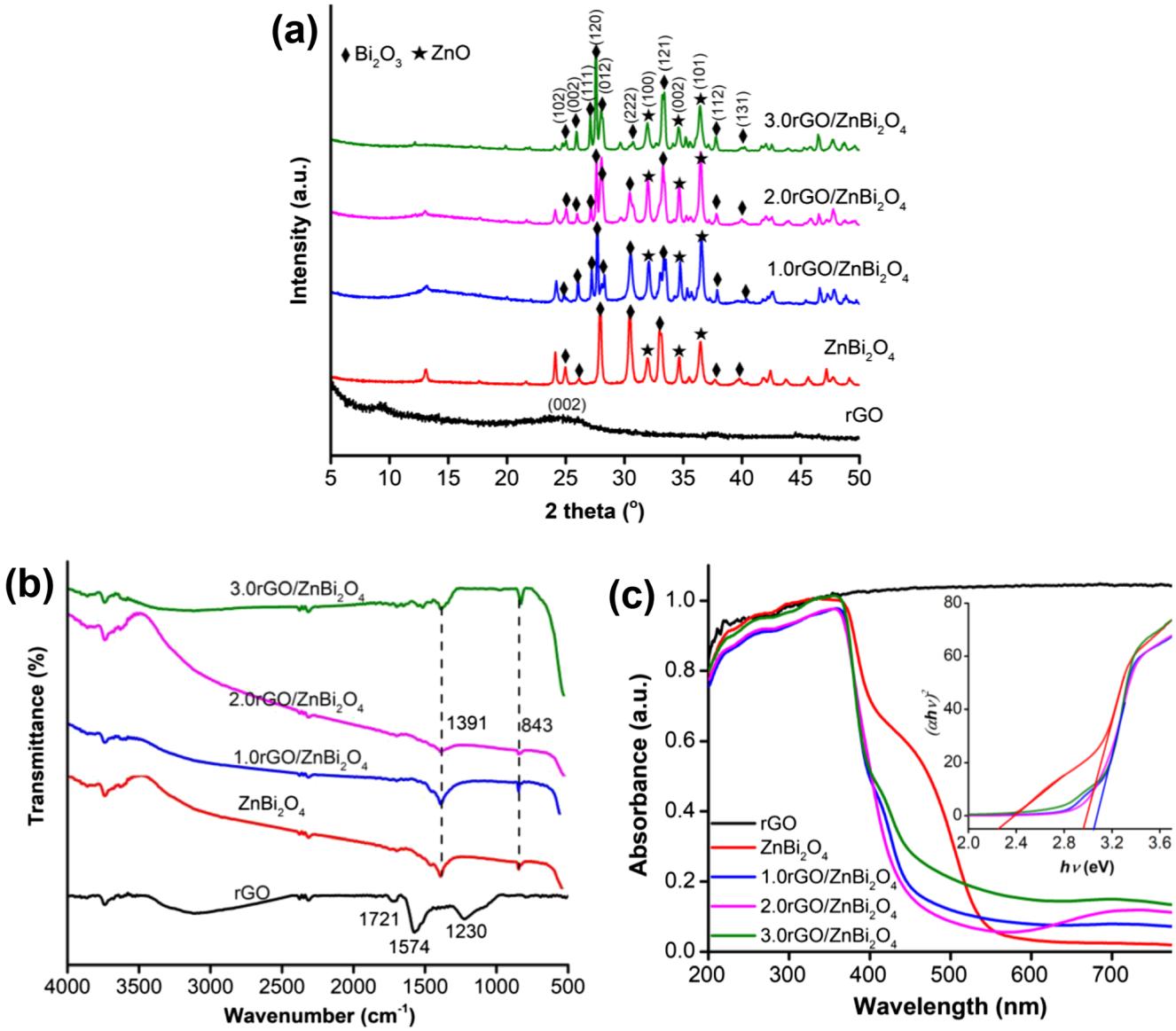

Fig. 1 **a** XRD pattern; **b** FTIR spectra, and **c** UV-Vis DRS spectra of as-prepared samples

Raman spectroscopy was used to further study the carbon structure of the rGO-$ZnBi_2O_4$. As shown in Fig. 3a, there were two characteristic peaks at 1331.9 and 1590.6 cm^{-1}, corresponding to the D and G bands, respectively. The D band was attributed to defects and edges of the rGO sheets, whereas the G band originated from the conjugated domains of sp^2-hybridized carbons. The 2D band of rGO-$ZnBi_2O_4$ also recorded around 2676 cm^{-1}, which corresponded to the single-layer characteristic of the rGO sheets (Akhavan et al. 2012).

The surface elemental composition and chemical states of Zn, Bi, O, and C in rGO/$ZnBi_2O_4$ were investigated by X-ray photoelectron spectroscopy (XPS), as shown in Fig. 3. As seen in Fig. 3c, the C1*s* XPS spectra of 2.0rGO/$ZnBi_2O_4$ show that the number of deconvoluted peaks were found at the binding energies of 284.6, 286.2, and 288.3 eV, corresponding to C–C/C=C, C–OH, and C=O bonds, respectively (Akhavan 2015; Akhavan et al. 2012; Cheng et al. 2019; Ma et al. 2019). This confirms the effective reduction of organic carbon in the 2.0rGO/$ZnBi_2O_4$ hybrid during the preparation process (Wu et al. 2012).

The Zn2*p* XPS spectrum of the $ZnBi_2O_4$ sample exhibited a peak at 1021.4 eV, denoting the presence of the main ZnO phase. However, a 0.4 eV shift to a lower binding energy of 1021.0 eV was observed for the 2.0rGO/$ZnBi_2O_4$ sample (Fig. 3d).

The XPS spectrum of Bi4f showed a peak at a binding energy of 159.1 eV for pristine $ZnBi_2O_4$ and 158.3 eV for the 2.0rGO/$ZnBi_2O_4$ sample. The Bi4*f* peak in the XPS spectrum of the 2.0rGO/$ZnBi_2O_4$ sample exhibited a 0.8 eV shift to lower binding energies, compared with that of pristine $ZnBi_2O_4$ (Fig. 3e). The O1*s* spectrum of the $ZnBi_2O_4$ sample displayed a peak at 530.3 eV, often found for metal-oxygen

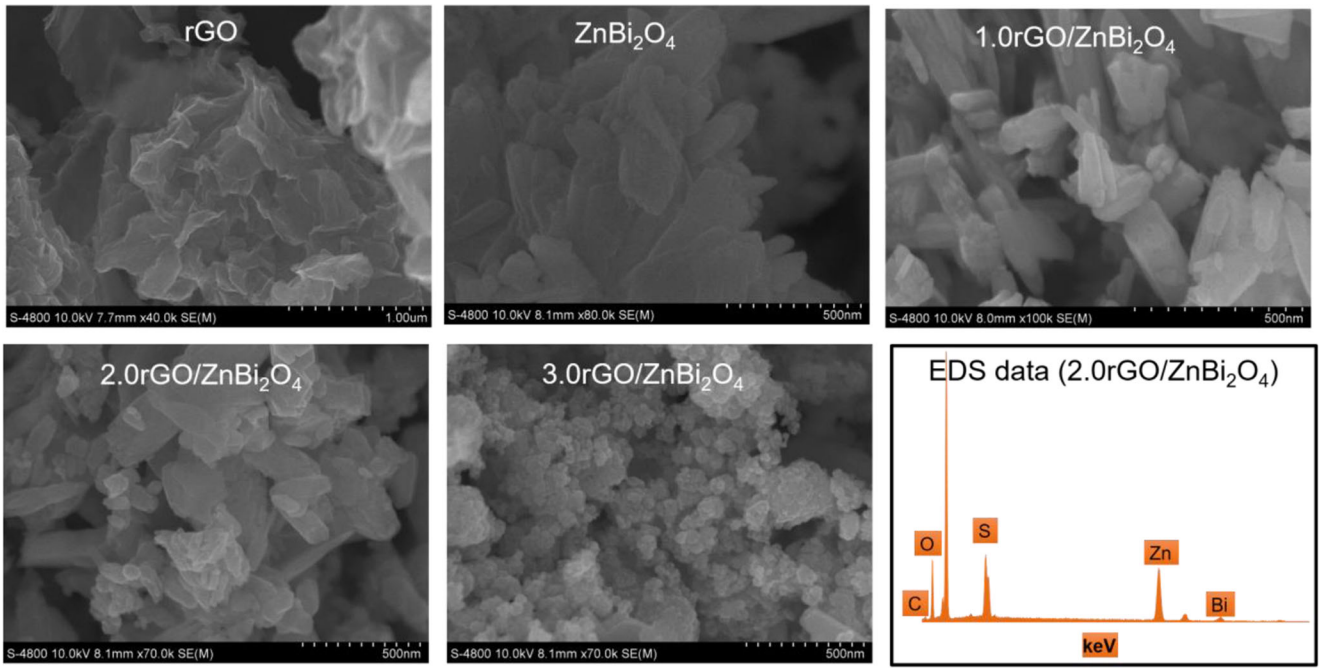

Fig. 2 SEM image and EDS of as-prepared samples

bonds. In the case of the 2.0rGO/$ZnBi_2O_4$ sample, the peak appeared at 529.9 eV, with a downshift of about 0.4 eV compared with the corresponding binding energy of pristine $ZnBi_2O_4$ (Fig. 3f). The reduction in binding energy for 2.0rGO/$ZnBi_2O_4$ confirms the charge transfer at the junction between rGO and $ZnBi_2O_4$.

Photocatalytic activity

The photocatalytic activity of the rGO/$ZnBi_2O_4$ hybrid samples was assessed by monitoring the degradation of 2,4-D, which is a hazardous herbicide extensively used for the control of broadleaf weeds. The experiments were carried out with an initial 2,4-D concentration of 30 mg/L, at pH 2.45, and using different catalysts with a concentration of 1.0 g/L. Figure 4a shows the photodegradation of 2,4-D under visible light irradiation on the pristine rGO and $ZnBi_2O_4$ samples, as well as on rGO/$ZnBi_2O_4$ hybrid catalysts with different rGO content. The photodegradation process followed a typical first-order kinetics, which can be expressed as $\ln(C_0/C_t) = kt$, where t is the reaction time (min), k is the degradation rate constant (min^{-1}), and C_0 and C_t are the concentrations of 2,4-D (mg/L) at $t = 0$ and t, respectively. As shown in Fig. 4b, the rate constant k corresponds to the slope of the linear fit of the $\ln(C_0/C_t)$ vs. t plot. A control experiment was performed under the same photocatalytic conditions; obviously, no self-degradation of 2,4-D was observed under visible light irradiation for 120 min. By introducing pristine rGO and $ZnBi_2O_4$, the 2,4-D degradation rate increased to 24.1 and 65.7%, respectively. However, the rGO/$ZnBi_2O_4$ hybrid catalysts showed superior photocatalytic activities to those of single-component pristine rGO and $ZnBi_2O_4$, although the photocatalytic activity of 3.0rGO/$ZnBi_2O_4$ was significantly lower than that of pristine $ZnBi_2O_4$. The photocatalytic activity of the rGO/$ZnBi_2O_4$ sample increased with increasing rGO content; however, the rate of photodegradation decreased when the content of rGO was further increased. This change in the photocatalytic activity of the rGO/$ZnBi_2O_4$ hybrid catalysts under visible light irradiation may be attributed to the following causes: first, a higher rGO content creates a higher number of photoinduced electron-hole pairs; second, an excessive rGO content may generate recombination centers for the photoinduced electron-hole pairs, or reduce the efficiency of the heterogeneous interfaces in the rGO/$ZnBi_2O_4$ sample, hindering charge transfer at these interfaces. Due to the charge transfer, the photocatalytic activity of rGO/$ZnBi_2O_4$ hybrid first increased and then decreased with increasing rGO content. The 2.0rGO/$ZnBi_2O_4$ exhibited the highest photocatalytic activity: about 90.0% of the 2,4-D content was degraded after 120 min of visible light irradiation. On the other hand, the photocatalytic activities of 1.0rGO/$ZnBi_2O_4$ and 3.0rGO/$ZnBi_2O_4$ samples were about 74.0 and 51.2%, respectively. The k value of the 2.0rGO/$ZnBi_2O_4$ sample was 0.0147 min^{-1}, which is higher than those of pristine rGO (6.7-fold increase), pristine $ZnBi_2O_4$ (1.8-fold), 1.0rGO/$ZnBi_2O_4$ (1.4-fold), and 3.0rGO/$ZnBi_2O_4$ (2.7-fold). The rGO component clearly enhanced the photocatalytic activity of $ZnBi_2O_4$; the interaction between rGO and $ZnBi_2O_4$ is a prerequisite for the synergistic effects that improve the efficiency of their heterogeneous interfaces, which play a major role in increasing the photocatalytic activity of the heterojunctions.

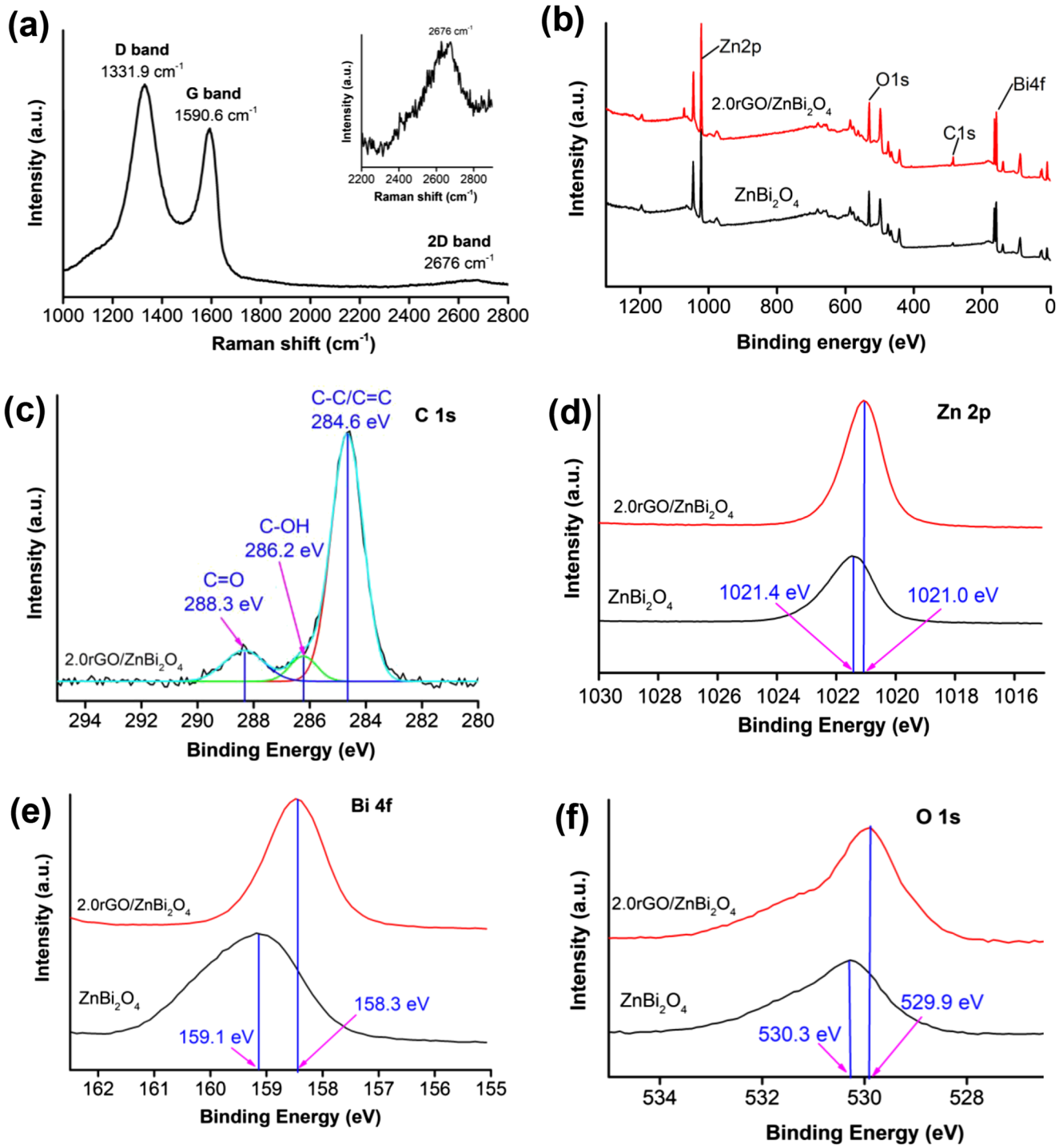

Fig. 3 **a** Raman spectra of 2.0rGO/$ZnBi_2O_4$ sample; XPS spectra **b** survey; **c** C 1 *s* **d** Zn 2*p*; **e** Bi 4*f*; and **f** O 1 *s* recorded for pristine $ZnBi_2O_4$ and 2.0rGO/$ZnBi_2O_4$ samples

Few studies have investigated the 2,4-D degradation activity of different catalysts. For instance, it has been reported that complete photodegradation of a 0.9 mmol/L solution of 2,4-D took place in 5 h with 1 wt.% TiO_2 supported on HY zeolite, using 2 g of catalyst per liter of solution (Shankar et al. 2006). Hexagonal mesoporous silica modified with copper phthalocyanines was able to degrade 90% of 0.05 mmol/L 2,4-D in 60 min, by adding 1.2 wt.% H_2O_2 and 0.5 g/L of catalyst (DeOliveira et al. 2008). The ferric sulfate/H_2O_2 system under UV irradiation has also been tested for the degradation of 2,4-D. The results showed that almost 100% of a 100 mg/L aqueous solution of 2,4-D was degraded using a Fe^{3+} concentration of 3 mg/L after 180 min of visible light irradiation (Conte et al. 2014). Furthermore, 83% of a 100 mg/L 2,4-D solution was

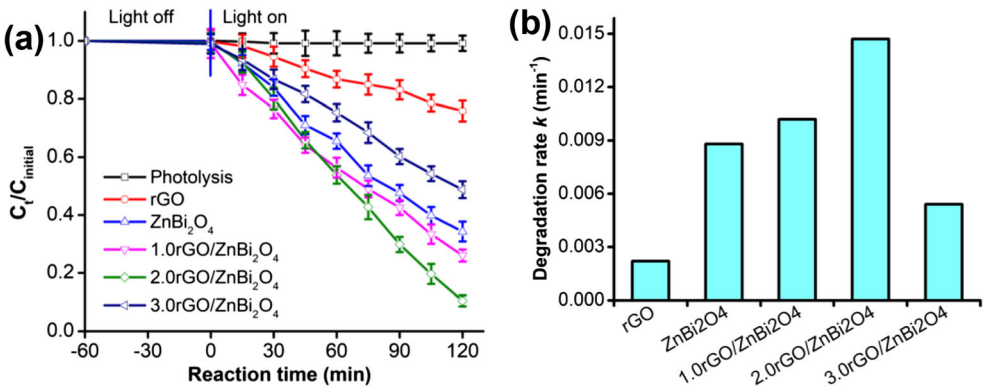

Fig. 4 **a** Photocatalytic activity and **b** photodegradation rate of as-prepared samples after 120 min visible light irradiation (catalyst 1.0 g/L, 2,4-D 30 mg/L at pH 2.45)

successfully degraded using a TiO_2@$MgFe_2O_4$ core-shell catalyst after 240 min of visible light irradiation in the presence of 7.20 mmol/L H_2O_2 (Huy et al. 2017a).

The effect of the 2.0rGO/$ZnBi_2O_4$ amount on the degradation of 2,4-D under visible light irradiation was investigated by varying the 2.0rGO/$ZnBi_2O_4$ concentration from 0.5 to 2.0 g/L, keeping the concentration of 2,4-D at 30 mg/L at pH 2.45; the results are shown in Fig. 5a. The photodegradation rate of 2,4-D increased from 0.0101 to 0.0147 min^{-1} when the 2.0rGO/$ZnBi_2O_4$ amount increased from 0.5 to 1.0 g/L. However, upon further increasing the amount of 2.0rGO/$ZnBi_2O_4$, the k value slightly decreased to 0.0143 min^{-1} for 1.5 g/L and 0.0142 min^{-1} for 2.0 g/L. This may be due to excessive amounts of 2.0rGO/$ZnBi_2O_4$ causing turbidity of the solution, which would prevent light transmission and hinder the degradation of 2,4-D.

The effect of the initial 2,4-D concentration on the degradation kinetics was investigated in the 2,4-D concentration range from 10 to 50 mg/L, with 1.0 g/L of 2.0rGO/$ZnBi_2O_4$ at pH 2.45. As shown in Fig. 5b, the 2,4-D degradation constant sharply decreased from 0.0516 to 0.0041 min^{-1} when the initial 2,4-D concentration increased from 10 to 50 mg/L. This can be explained by the fact that, at high concentrations of 2,4-D, a given amount of 2.0rGO/$ZnBi_2O_4$ cannot produce enough active species to oxidize 2,4-D, leading to a reduced photodegradation efficiency. The highest degradation of 2,4-D was observed at an initial 2,4-D concentration of 30 mg/L, when approximately 90% of 2,4-D was degraded after 120 min of visible light irradiation.

The effect of the pH on the photodegradation activity of the catalysts was investigated by varying the pH of the 2,4-D solution in the 1.0–7.0 range, keeping the initial 2,4-D concentration at 30 mg/L and the 2.0rGO/$ZnBi_2O_4$ concentration at 1.0 g/L; the results are shown in Fig. 5c. After 120 min of irradiation, the percentages of 2,4-D degradation at pH 1.0, 2.45, 4.0, and 7.0 were 64, 90, 56, and 24%, respectively. It is well known that the carboxyl group of 2,4-D is protonated in solution, and the surface of $ZnBi_2O_4$ contains a large number of positively charged sites. Moreover, the interaction between 2,4-D and the surface of 2.0rGO/$ZnBi_2O_4$ is mainly controlled by the electrostatic attraction or repulsion between the 2,4-D form in solution and the surface. The reduced degradation of 2,4-D at pH values lower or higher than 2.45 could be explained as follows: at pH 1.0, because high H^+ concentration in solution inhibited the protonation of 2,4-D, while at pH 4.0 and 7.0 the higher concentrations of OH^- species in solution competed with the 2,4-D anion, preventing its contact with 2.0rGO/$ZnBi_2O_4$, thus hindering the degradation of 2,4-D.

In order to investigate the stability of the photocatalytic performance under visible light irradiation, a 2,4-D photodegradation test was repeated for four consecutive cycles. The experiments were carried out with an initial 2,4-D concentration of 30 mg/L, at pH 2.45, and using 2.0rGO/$ZnBi_2O_4$ with a catalyst/2,4-D solution ratio of 1.0 g/L. After each experiment, following centrifugation to separate it from the reaction solution, the 2.0rGO/$ZnBi_2O_4$ catalyst was rinsed and dried. The dried 2.0rGO/$ZnBi_2O_4$ catalyst was then reused in the subsequent experiment. As shown in Fig. 5d, the photocatalyst exhibited good photostability under visible light irradiation, and its photocatalytic efficiency was reduced by only 7% after four repeated cycles. This demonstrates the good stability and recyclability of the 2.0rGO/$ZnBi_2O_4$ hybrid catalyst, which represent favorable features for practical applications.

To determine the mineralization ability of the catalyst, the total organic carbon (TOC) in solution before and after visible light irradiation of a 30 mg/L solution of 2,4-D was also measured at pH 2.45, using 2.0rGO/$ZnBi_2O_4$ with a catalyst/2,4-D solution ratio of 1.0 g/L. The TOC content in solution before and after visible light irradiation was estimated to be about 13.09 and 2.14 mg/L, respectively; therefore, the TOC removal efficiency of the 2.0rGO/$ZnBi_2O_4$ hybrid catalyst was 83.7% after 120 min of visible light irradiation. Conte's group reported that the homogeneous catalysis mineralization of 2,4-D in the ferric sulfate/H_2O_2 system under UV irradiation only reached 55% after 180 min, using 100 mg/L of 2,4-D (Conte et al. 2014). The degree of 2,4-D dechlorination was determined by measuring the concentration of inorganic chloride in solution after 120 min of visible light irradiation. The concentration of chloride corresponding to the initial 2,4-D concentration in solution was

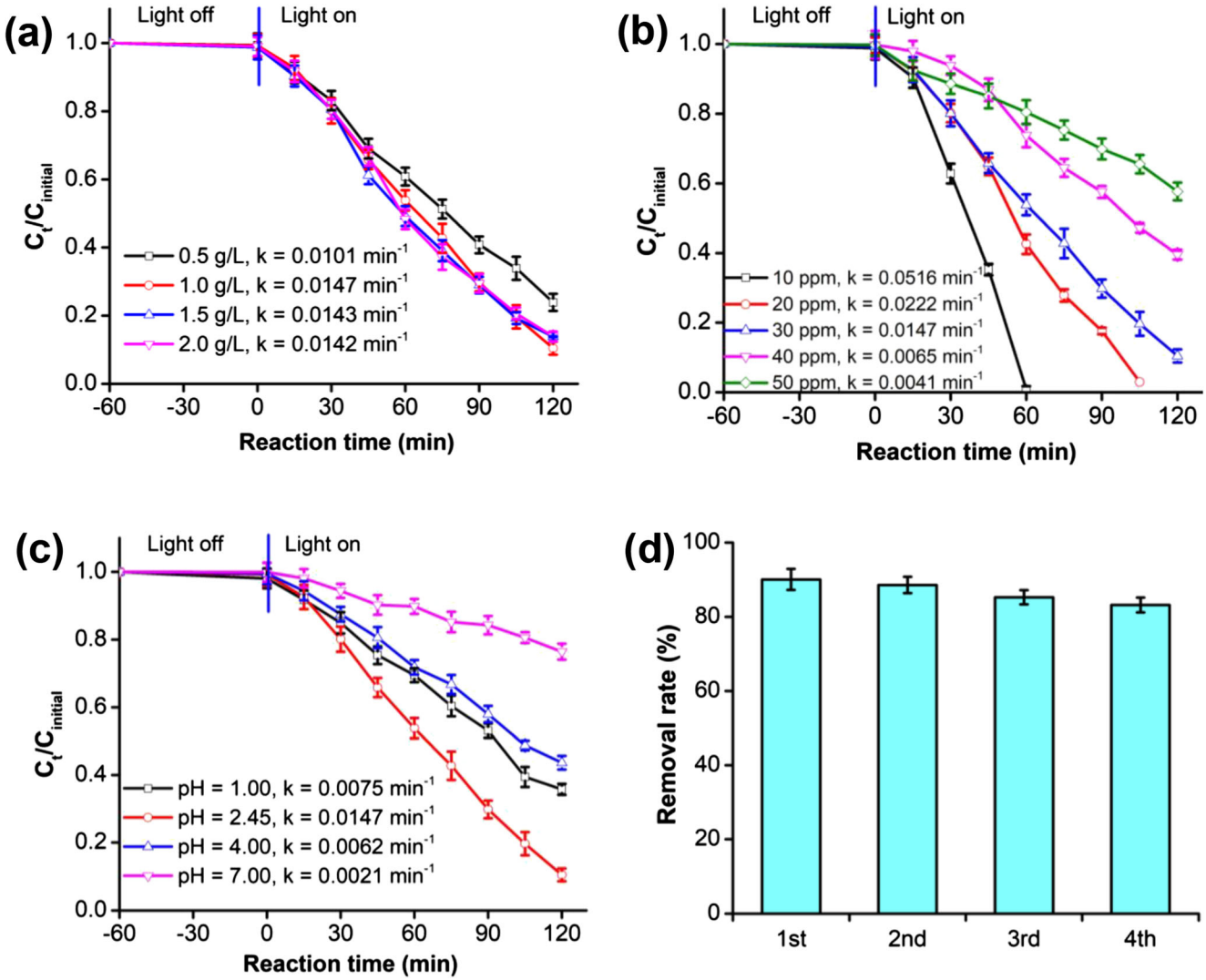

Fig. 5 **a** Effect of quantity of 2.0rGO/$ZnBi_2O_4$ hybrid catalyst; **b** effect of initial 2,4-D concentration, **c** effect of pH solution, and **d** recycle performance tests for the visible light degradation of 2,4-D using by 2.0rGO/$ZnBi_2O_4$

9.66 mg/L. A 8.53 mg/L concentration of inorganic chloride was generated after 120 min of visible light irradiation, which highlights the very high 2,4-D dechlorination efficiency (~ 88.3%) of the 2.0rGO/$ZnBi_2O_4$ catalyst.

Trapping experiments and proposed photodegradation mechanism of hybrid catalyst

To investigate the possible role of active species in the photocatalytic degradation, a series of trapping agents such as *tert*-butanol (2 mmol/L), *p*-benzoquinone (2 mmol/L), disodium ethylenediaminetetraacetic acid (Na_2EDTA, 1 mmol/L), and $AgNO_3$ (1 mmol/L) were used in trapping experiments. The tests were performed with an initial 2,4-D concentration of 30 mg/L, at pH 2.45, and using 2.0rGO/$ZnBi_2O_4$ with a catalyst/2,4-D solution ratio of 1.0 g/L. Figure 6a shows the photocatalytic activity of 2.0rGO/$ZnBi_2O_4$ for the degradation of 2,4-D under visible light irradiation, with or without trapping agents.

The photodegradation activity of 2.0rGO/$ZnBi_2O_4$ decreased with the addition of *tert*-butanol ($OH^•$ radical trapper): approximately 38.9% of 2,4-D was degraded after 120 min of visible light irradiation, confirming that the $OH^•$ radical is not the main active species. After Na_2EDTA (photoinduced h^+ acceptor) was added into the system, the photocatalytic activity of 2.0rGO/$ZnBi_2O_4$ showed a significant decrease. The degradation efficiency of 2,4-D dropped to 8.8% after visible light irradiation for 120 min, suggesting that the photoinduced h^+ species play a major role in the 2,4-D photodegradation process. Notably, about 16.6% of 2,4-D was degraded when *p*-benzoquinone ($O_2^{•-}$ radical trapper) was added into the system, which means that the $O_2^{•-}$ radical also plays an important role in 2,4-D photodegradation process. The 2,4-D degradation efficiency slightly increased to 94.2% after 120 min of visible light irradiation upon addition of $AgNO_3$ (photoinduced e^-

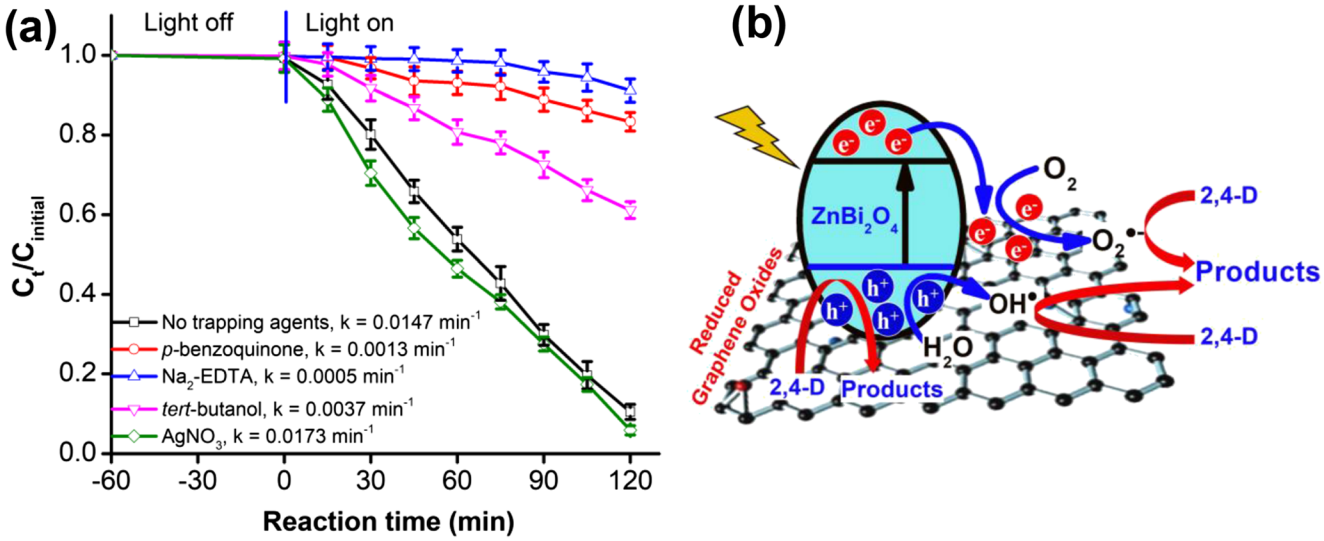

Fig. 6 **a** Photocatalytic activity of 2.0rGO/$ZnBi_2O_4$ for the degradation of 2,4-D with and without adding reactive species trapping agents after 120 min visible light irradiation and **b** proposed mechanism for the photoinduced e^--h^+ separation and transport at the visible light driven 2.0rGO/$ZnBi_2O_4$ hybrid catalyst interface

acceptor); this indicates that the recombination of photoinduced e^--h^+ pairs in 2.0rGO/$ZnBi_2O_4$ is negligible. The results of the active species trapping experiments thus demonstrate that $O_2^{\bullet-}$ and h^+ (but not the OH• radical) are the main active species in the photocatalytic degradation of 2,4-D .

Based on the results of the experiments, we propose the photocatalytic mechanism of 2.0rGO/$ZnBi_2O_4$ shown in Fig. 6b. Under visible light irradiation, $ZnBi_2O_4$ excites and produces photoinduced e^--h^+ pairs; subsequently, the photoinduced e^- species immediately move from $ZnBi_2O_4$ to rGO. As is well known, the photoinduced e^- can effectively reduce O_2 molecules adsorbed on the surface of 2.0rGO/$ZnBi_2O_4$ to generate $O_2^{\bullet-}$ radicals, which are among the most important active species in the degradation system. In addition, the photoinduced h^+ can oxidize 2,4-D or react with H_2O to generate OH• radicals. The generated OH• and $O_2^{\bullet-}$ radicals can then oxidize 2,4-D. Therefore, the rapid scavenging of photoinduced electrons by rGO (acting as electron acceptor in the hybrid catalyst) is likely to prevent direct photoinduced e^--h^+ recombination, enhancing the photocatalytic activity.

The photodegradation mechanism of 2,4-D by the rGO/$ZnBi_2O_4$ can be described by the following reactions:

$$ZnBi_2O_4 + h\nu \rightarrow ZnBi_2O_4\ (e^-, h^+) \quad (1)$$

$$e^- + \text{rGO} \rightarrow \text{rGO}\ (e^-) \quad (2)$$

$$\text{rGO}\ (e^-) + O_2 \rightarrow O_2^{\bullet-} \quad (3)$$

$$ZnBi_2O_4\ (h^+) + 2H_2O \rightarrow OH^{\bullet} + H^+ \quad (4)$$

$$ZnBi_2O_4\ (h^+) + 2,4\text{–D} \rightarrow \text{degradation products} \rightarrow CO_2 + H_2O \quad (5)$$

$$O_2^{\bullet-} + 2,4\text{–D} \rightarrow \text{degradation products} \rightarrow CO_2 + H_2O \quad (6)$$

$$OH^{\bullet} + 2,4\text{–D} \rightarrow \text{degradation products} \rightarrow CO_2 + H_2O \quad (7)$$

$$h^+ + e^- \rightarrow (e^-, h^+)\ \text{(negligible recombination)} \quad (8)$$

Conclusions

A new highly efficient rGO/$ZnBi_2O_4$ hybrid catalyst has been successfully synthesized by oxidation-reduction and co-precipitation methods, followed by heating at 450 °C. The toxic organic pollutant 2,4-D has been shown to undergo degradation in aqueous solution under visible light irradiation of rGO/$ZnBi_2O_4$. The improved photocatalytic activity of the rGO/$ZnBi_2O_4$ hybrid catalyst might be due to the presence of rGO. The latter served as an excellent e^- acceptor and mediator in the hybrid catalyst, enhancing the migration of photoinduced e^- and hindering the recombination of photoinduced e^--h^+ pairs. A possible 2,4-D degradation mechanism by the rGO/$ZnBi_2O_4$ catalyst under visible light was also proposed. The 2.0rGO/$ZnBi_2O_4$ catalyst led to 90% degradation of 2,4-D (with $k = 0.0147\ min^{-1}$) after 120 min of visible light irradiation. In addition, 2.0rGO/$ZnBi_2O_4$ displayed excellent stability in four successive cycles. Therefore, the present rGO/$ZnBi_2O_4$ catalyst shows great potential for application in the oxidative removal of persistent organic pollutants.

Funding information This research is funded by Vietnam National Foundation for Science and Technology Development (NAFOSTED) under grant number 104.05-2017.29.

References

Akhavan O (2015) Bacteriorhodopsin as a superior substitute for hydrazine in chemical reduction of single-layer graphene oxide sheets. Carbon 81:158–166. https://doi.org/10.1016/j.carbon.2014.09.044

Akhavan O, Ghaderi E (2009) Photocatalytic reduction of graphene oxide nanosheets on TiO2 thin film for photoinactivation of bacteria in solar light irradiation. J Phys Chem C 113:20214–20220. https://doi.org/10.1021/jp906325q

Akhavan O, Ghaderi E, Akhavan A (2012) Size-dependent genotoxicity of graphene nanoplatelets in human stem cells. Biomaterials 33:8017–8025. https://doi.org/10.1016/j.biomaterials.2012.07.040

An J, Zhu L, Zhang Y, Tang H (2013) Efficient visible light photo-Fenton-like degradation of organic pollutants using in situ surface-modified BiFeO3 as a catalyst. J Environ Sci 25:1213–1225. https://doi.org/10.1016/S1001-0742(12)60172-7

An X, Liu H, Qu J, Moniz SJA, Tang J (2015) Photocatalytic mineralisation of herbicide 2,4,5-trichlorophenoxyacetic acid: enhanced performance by triple junction Cu–TiO2–Cu2O and the underlying reaction mechanism. New J Chem 39:314–320. https://doi.org/10.1039/c4nj01317d

Cao J, Xu B, Lin H, Luo B, Chen S (2012) Novel Bi2S3-sensitized BiOCl with highly visible light photocatalytic activity for the removal of rhodamine B. Catal Commun 26:204–208. https://doi.org/10.1016/j.catcom.2012.05.025

Cheng C, Jia P, Xiao L, Geng J (2019) Tandem chemical modification/mechanical exfoliation of graphite: scalable synthesis of high-quality, surface-functionalized graphene. Carbon 145:668–676. https://doi.org/10.1016/j.carbon.2019.01.079

Cheng L, Kang Y (2014) Selective preparation of Bi2O3 visible light-driven photocatalyst by dispersant and calcination. J Alloys Compd 585:85–93. https://doi.org/10.1016/j.jallcom.2013.08.010

Conte LO, Querini P, Albizzati ED, Alfano OM (2014) Photonic and quantum efficiencies for the homogeneous photo-Fenton degradation of herbicide 2,4-D using different iron complexes. J Chem Technol Biotechnol 89:1967–1974. https://doi.org/10.1002/jctb.4284

DeOliveira E et al (2008) Hexagonal mesoporous silica modified with copper phthalocyanine as a photocatalyst for pesticide 2,4-dichlorophenoxiacetic acid degradation. J Colloid Interface Sci 323:98–104. https://doi.org/10.1016/j.jcis.2008.04.025

Gadhi TA et al (2018) Single BiFeO3 and mixed BiFeO3/Fe2O3/Bi2Fe4O9 ferromagnetic photocatalysts for solar light driven water oxidation and dye pollutants degradation. J Ind Eng Chem 63:437–448. https://doi.org/10.1016/j.jiec.2018.03.004

Goh K-H, Lim T-T, Dong Z (2008) Application of layered double hydroxides for removal of oxyanions: a review. Water Res 42:1343–1368. https://doi.org/10.1016/j.watres.2007.10.043

Goswami K, Ananthakrishnan R (2017) Facile synthesis of nano-Zn/Bi–reduced graphene oxide for enhanced photocatalytic elimination of chlorinated organic pollutants under visible light. New J Chem 41:4406–4415. https://doi.org/10.1039/c7nj00996h

Hummers WS, Offeman RE (1958) Preparation of graphitic oxide. J Am Chem Soc 80:1339–1339. https://doi.org/10.1021/ja01539a017

Huy BT, Jung D-s, Kim Phuong NT, Lee Y-I (2017a) Enhanced photodegradation of 2,4-dichlorophenoxyacetic acid using a novel TiO2@MgFe2O4 core@shell structure. Chemosphere 184:849–856. https://doi.org/10.1016/j.chemosphere.2017.06.069

Huy BT, Paeng DS, Thi Bich Thao C, Kim Phuong NT, Lee Y-I (2019) ZnO-Bi2O3/graphitic carbon nitride photocatalytic system with H2O2-assisted enhanced degradation of Indigo carmine under visible light. Arab J Chem. https://doi.org/10.1016/j.arabjc.2019.01.003

Huy BT, Thao CTB, Dao V-D, Phuong NTK, Lee Y-I (2017b) A mixed-metal oxides/graphitic carbon nitride: high visible light photocatalytic activity for efficient mineralization of rhodamine B. Adv Mater Interfaces 4:1700128. https://doi.org/10.1002/admi.201700128

Ju P, Wang P, Li B, Fan H, Ai S, Zhang D, Wang Y (2014) A novel calcined Bi2WO6/BiVO4 heterojunction photocatalyst with highly enhanced photocatalytic activity. Chem Eng J 236:430–437. https://doi.org/10.1016/j.cej.2013.10.001

Kumar R et al (2015) Bulk synthesis of highly conducting graphene oxide with long range ordering. RSC Adv 5:35893–35898. https://doi.org/10.1039/c5ra01943e

Liu L, Jiang J, Jin S, Xia Z, Tang M (2011a) Hydrothermal synthesis of β-bismuth oxide nanowires from particles. CrystEngComm 13:2529–2532. https://doi.org/10.1039/c0ce00773k

Liu X, Pan L, Lv T, Lu T, Zhu G, Sun Z, Sun C (2011b) Microwave-assisted synthesis of ZnO–graphene composite for photocatalytic reduction of Cr(vi). Cat Sci Technol 1:1189–1193. https://doi.org/10.1039/c1cy00109d

Ma J et al (2019) Covalent confinement of sulfur copolymers onto graphene sheets affords ultrastable lithium–sulfur batteries with fast cathode kinetics. ACS Appl Mater Interfaces 11:13234–13243. https://doi.org/10.1021/acsami.9b00214

Martínez-Huitle CA, Ferro S (2006) Electrochemical oxidation of organic pollutants for the wastewater treatment: direct and indirect processes. Chem Soc Rev 35:1324–1340. https://doi.org/10.1039/b517632h

Meng D et al (2014) A dual-fluorescent composite of graphene oxide and poly(3-hexylthiophene) enables the ratiometric detection of amines. Chem Sci 5:3130–3134. https://doi.org/10.1039/C4SC00598H

Mishra G, Dash B, Pandey S (2018) Layered double hydroxides: a brief review from fundamentals to application as evolving biomaterials. Appl Clay Sci 153:172–186. https://doi.org/10.1016/j.clay.2017.12.021

Mohapatra L, Parida K (2016) A review on the recent progress, challenges and perspective of layered double hydroxides as promising photocatalysts. J Mater Chem A 4:10744–10766. https://doi.org/10.1039/C6TA01668E

Pei S, Zhao J, Du J, Ren W, Cheng H-M (2010) Direct reduction of graphene oxide films into highly conductive and flexible graphene films by hydrohalic acids. Carbon 48:4466–4474. https://doi.org/10.1016/j.carbon.2010.08.006

Peng Y, Yan M, Chen Q-G, Fan C-M, Zhou H-Y, Xu A-W (2014) Novel one-dimensional Bi2O3–Bi2WO6 p–n hierarchical heterojunction with enhanced photocatalytic activity. J Mater Chem A 2:8517–8524. https://doi.org/10.1039/c4ta00274a

Ponraj C, Vinitha G, Daniel J (2017) A review on the visible light active BiFeO3 nanostructures as suitable photocatalyst in the degradation of different textile dyes. Environ Nanotechnol Monit Manag 7:110–120. https://doi.org/10.1016/j.enmm.2017.02.001

Shankar MV, Anandan S, Venkatachalam N, Arabindoo B, Murugesan V (2006) Fine route for an efficient removal of 2,4-dichlorophenoxyacetic acid (2,4-D) by zeolite-supported TiO2. Chemosphere 63:1014–1021. https://doi.org/10.1016/j.chemosphere.2005.08.041

Shekofteh-Gohari M, Habibi-Yangjeh A (2016) Novel magnetically separable ZnO/AgBr/Fe3O4/Ag3VO4 nanocomposites with tandem n–n heterojunctions as highly efficient visible-light-driven photocatalysts. RSC Adv 6:2402–2413. https://doi.org/10.1039/c5ra21356h

Sun J, Xiao L, Meng D, Geng J, Huang Y (2013) Enhanced photoresponse of large-sized photoactive graphene composite films based on water-soluble conjugated polymers. Chem Commun 49:5538–5540. https://doi.org/10.1039/C3CC40563J

Thi Mai Tho N, The Huy B, Nha Khanh DN, Quoc Thang N, Thi Phuong Dieu N, Dai Duong B, Thi Kim Phuong N (2018) Mechanism of visible-light photocatalytic mineralization of indigo carmine using

ZnBi2O4-Bi2S3 composites. ChemistrySelect 3:9986–9994. https://doi.org/10.1002/slct.201802151

Tho NTM et al (2018) Facile synthesis of ZnBi2O4-graphite composites as highly active visible-light photocatalyst for the mineralization of rhodamine B. Korean J Chem Eng 35:2442–2451. https://doi.org/10.1007/s11814-018-0156-z

Tokunaga S, Kato H, Kudo A (2001) Selective preparation of monoclinic and tetragonal BiVO4 with scheelite structure and their photocatalytic properties. Chem Mater 13:4624–4628. https://doi.org/10.1021/cm0103390

Wang J et al (2017) Preparation of Bi2S3/carbon quantum dot hybrid materials with enhanced photocatalytic properties under ultraviolet-, visible- and near infrared-irradiation. Nanoscale 9:15873–15882. https://doi.org/10.1039/c7nr04593j

Wang Y et al (2014) Electrostatic self-assembly of BiVO4–reduced graphene oxide nanocomposites for highly efficient visible light photocatalytic activities. ACS Appl Mater Interfaces 6:12698–12706. https://doi.org/10.1021/am502700p

Wang YR, Chu W (2012) Photo-assisted degradation of 2,4,5-trichlorophenoxyacetic acid by Fe(II)-catalyzed activation of oxone process: the role of UV irradiation, reaction mechanism and mineralization. Appl Catal B Environ 123-124:151–161. https://doi.org/10.1016/j.apcatb.2012.04.031

Wu L, Bi J, Li Z, Wang X, Fu X (2008) Rapid preparation of Bi2WO6 photocatalyst with nanosheet morphology via microwave-assisted solvothermal synthesis. Catal Today 131:15–20. https://doi.org/10.1016/j.cattod.2007.10.089

Wu N, She X, Yang D, Wu X, Su F, Chen Y (2012) Synthesis of network reduced graphene oxide in polystyrene matrix by a two-step reduction method for superior conductivity of the composite. J Mater Chem 22:17254–17261. https://doi.org/10.1039/c2jm33114d

Xu Z, Tabata I, Hirogaki K, Hisada K, Wang T, Wang S, Hori T (2012) UV-induced formation of activated Bi2O3 nanoflake: an enhanced visible light driven photocatalyst by platinum loading. RSC Adv 2:103–106. https://doi.org/10.1039/C1RA00638J

Yang J, Wang X, Dai J, Li J (2014) Efficient visible-light-driven photocatalytic degradation with Bi2O3 coupling silica doped TiO2. Ind Eng Chem Res 53:12575–12586. https://doi.org/10.1021/ie501850m

Yao Y, Qin J, Cai Y, Wei F, Lu F, Wang S (2014) Facile synthesis of magnetic ZnFe2O4–reduced graphene oxide hybrid and its photo-Fenton-like behavior under visible iradiation. Environ Sci Pollut Res 21:7296–7306. https://doi.org/10.1007/s11356-014-2645-x

Yu J, Kudo A (2006) Effects of structural variation on the photocatalytic performance of hydrothermally synthesized BiVO4. Adv Funct Mater 16:2163–2169. https://doi.org/10.1002/adfm.200500799

Yuan B, Song L, Liew KM, Hu Y (2015) Solid acid-reduced graphene oxide nanohybrid for enhancing thermal stability, mechanical property and flame retardancy of polypropylene. RSC Adv 5:41307–41316. https://doi.org/10.1039/c5ra04699h

Zhao G, Liu S, Lu Q, Song L (2012) Controllable synthesis of Bi2WO6 nanofibrous mat by electrospinning and enhanced visible photocatalytic degradation performances. Ind Eng Chem Res 51:10307–10312. https://doi.org/10.1021/ie300988z

Zhong S, Zhang F, Lu W, Wang T, Qu L (2015) One-step synthesis of Bi2WO6/Bi2O3 loaded reduced graphene oxide multicomponent composite with enhanced visible-light photocatalytic activity. RSC Adv 5:68646–68654. https://doi.org/10.1039/c5ra08538a